Abrasive medium classification and CFD simulations for low-pressure abrasive water-jet blasting

Ekrem Özkaya*[a], Evren Bayraktar[b], Stefan Turek[b] and Dirk Biermann[a]

[a] Institute of Machining Technology, TU Dortmund
Baroper Straße 301, D-44227, Dortmund, Germany
[b] Institute of Applied Mathematics (LS III), TU Dortmund
Vogelpothsweg 87, D-44227, Dortmund, Germany

E-mail: oezkaya@isf.de

Abstract

This study concerns the determination of the significant factors for an innovative deburring process: low pressure abrasive water-jet blasting. We firstly classify the abrasive medium aluminum oxide (Al_2O_3) according to the individual characteristics of different grain sizes. Then, the particle behavior in the air jet is analyzed with an optical measuring method, Particle Image Velocimetry (PIV); the velocity profile and the particle distribution of the dispersed system are obtained. Computational Fluid Dynamics (CFD) simulations were verified by comparing the experimental and numerical results, and we could specify the velocity range for the abrasive particles.

Keywords: *abrasive particles, deburring, micro machining, Computational Fluid Dynamics, micro abrasive water-jet blasting*

Deutscher Abstrakt

Zur Realisierung eines Simulationsmodells, welches einen innovativen Entgratprozess durch Niederdruck-Abrasivwasserstrahlen für mikrostrukturierte Bauteile in der Entwicklung unterstützt, steht im Mittelpunkt der Untersuchungen zunächst die Ermittlung signifikanter Einflussgrößen. In diesem Beitrag werden daher als erstes die individuellen Eigenschaften unterschiedlicher Korngrößen des Abrasivmittels Aluminiumoxid (Al_2O_3) für den Prozess klassifiziert. Anschließend erfolgt die Beobachtung des Partikelverhaltens im Abrasivdruckluftstrahl mit einem optischen Messverfahren. Dabei werden der Geschwindigkeitsverlauf und die Partikelverteilung über die Strahlhöhe und -breite im dispersen System analysiert. Durch den abschließenden Vergleich der gewonnenen Ergebnisse kann der Gültigkeitsbereich der minimalen und maximalen Geschwindigkeitsfelder, in der sich die Partikel bewegen, begrenzt sowie die erreichte Simulationsgüte prognostiziert werden.

1 Introduction

The microsystem is a key technology with a great potential for innovation. Trends in the production technologies, namely multi-functionality and miniaturization, make the micro-deburring process even more important, which is required for finishing of microparts being made of high performance material, within a safe manufacturing process. Accordingly, there is a significant interest in the development and in the research of the micro deburring process as well in its industrial implementations.

The micro burrs remaining on the work piece are a major problem in the production of microparts, especially in micro machining; even though, it can be considered as the most flexible method. Most deburring methods, e.g. manual, mechanical or electrochemical methods, yield unsatisfactory results: Micro burrs still have remained after the finishing process.. The smaller the workpieces, the higher are the requirements to be met by the subsequent deburring process. In order to ensure the functional capability and cleanliness of micro workpieces, we have been developing a novel micro deburring process and an adaptive simulation model by investigating the relevant process parameters.

In contrast to numerous phenomenological investigations, there are almost no theoretical publications about the mechanisms in deburring of micro-workpieces consisting of materials which are hard to machine by using abrasive water-jet blasting, e.g. Nickel-Titanium shape memory alloys (NiTi-SMA). Moreover, there are very few mathematical modeling studies and almost no numerical studies on the deburring process. Another problem is the resolving the flow field and the description of physical interactions between the carrying and abrasive media. The problem partly arises on account of the limits of the optical measurement methods for the abrasive water jet, which is possible only with highly sophisticated experimental set-ups, e.g., Laser and Phase Doppler Anemometry (LDA, PDA) [Mea03]. The experiments with water jet under room conditions were extensively studied but no success was obtained [Baa96]. To establish the desired mathematical model is difficult due to being the low-pressure abrasive water jet realized within an injection method and having a free surface flow. Moreover, since the model cannot be purely formulated in a theoretical manner, the empirical lost coefficients and several other factors have to be taken into account [Him93, Baa96].

The mentioned challenges and the limitations in measurement methods motivated us to study the realization of the deburring process, CFD simulations and resolving the flow field of the abrasive-laden air jet. As a promising solution, the dispersed flow should be numerically simulated to obtain the velocity of the particles and their distribution. In order to make an accurate prediction of the flow field, experimental and numerical investigations were carried out for a free air jet; the velocity field of the jet is measured by using a laser optical measurement technique VisiSize Oxford Lasers Technology Typ N60. The measured data are compared against the results which are obtained with the empirical formula, equation (7); later, a numerical flow simulation was carried out, as well. The comparison of experimental and numerical results leads to conclusions on the behavior of abrasive air jet and also provides new insights and optimization ideas for the low-pressure micro abrasive waterjet blasting process.

2 Experiment

2.1 Analysis of particles

In order to determine a suitable abrasive medium for the deburring process, three different grain sizes, F150, F220 and F500 of aluminum oxide (Al_2O_3), according to FEPA (Fédération Européenne des Fabricants de Produits Abrasifs) were analyzed (*Table 1*). These types of abrasive particles are suitable for the deburring process due to its hardness and good removal properties.

Table 1: Analyzed abrasive particles

Name	Manufacturer´s specifications (µm)	Material	Hardness (Mohs)	Shape
F500	5 - 25	aluminum oxide	9	edged
F220	53 - 75	aluminum oxide	9	edged
F150	63 - 106	aluminum oxide	9	edged

The measured data were plotted in a graph for volume- and number-density distributions so to see the number density (q_0), the volume density (q_3) and their cumulative values (Q_0 ,Q_3) with respect to the particle size; the data are presented between D_{10} and D_{95} in *Figure 1, Figure 2* and *Figure 3*. Additionally, we could subjectively evaluate the particle character with the microscopic photography. A visual comparison of

the micro photographs shows that the F500 abrasive medium has a relatively irregular scattering, most probably due to the high porosity of the fine particles.

The median diameter D_{50} has a great importance for the analysis of particles. It is directly related to the mass and volumetric distributions which are the key variables for us, so we can decide that if the particles are sufficiently large, i.e. we can decide on whether the capillary action takes place or does not. The sum of volume distribution Q_3 can be calculated according to equation (1) and indicates the proportion of the particles that are less than or equal to a certain particle size x_i (interval limit x_i).

$$Q_3\{x_i\} = \frac{quantity\ of\ all\ particles\ with\ x\ \leq x_i}{Total\ quantity\ of\ all\ particles} \tag{1}$$

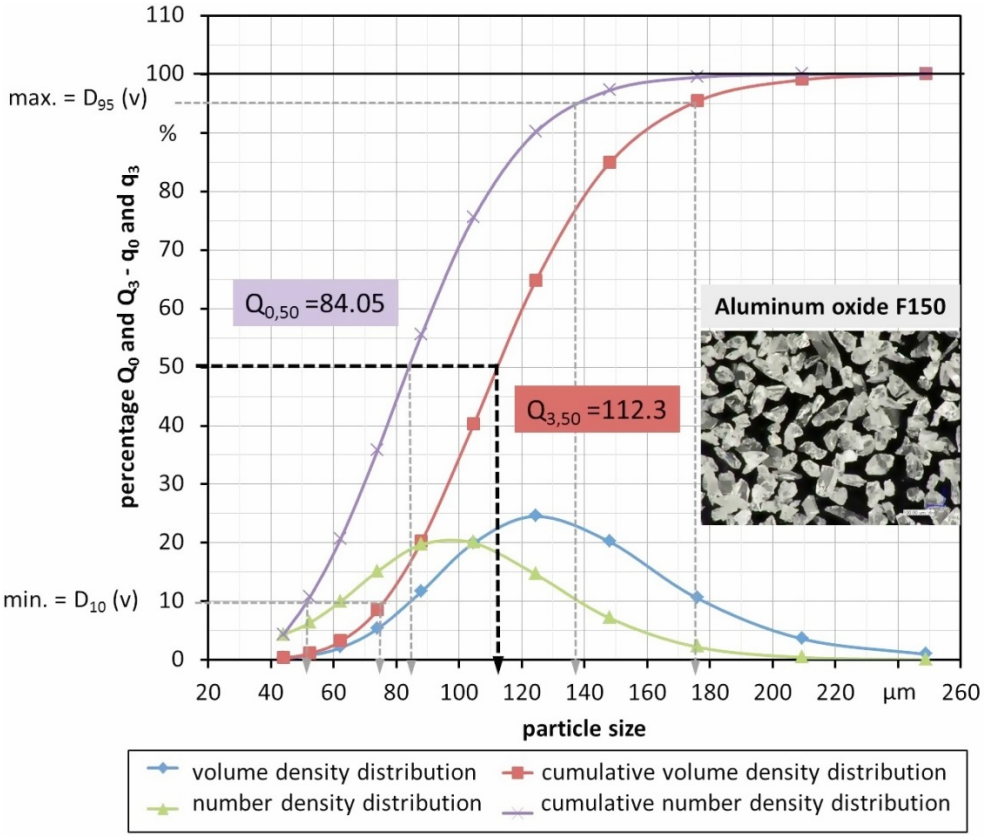

Figure 1: Number and volume distribution F150

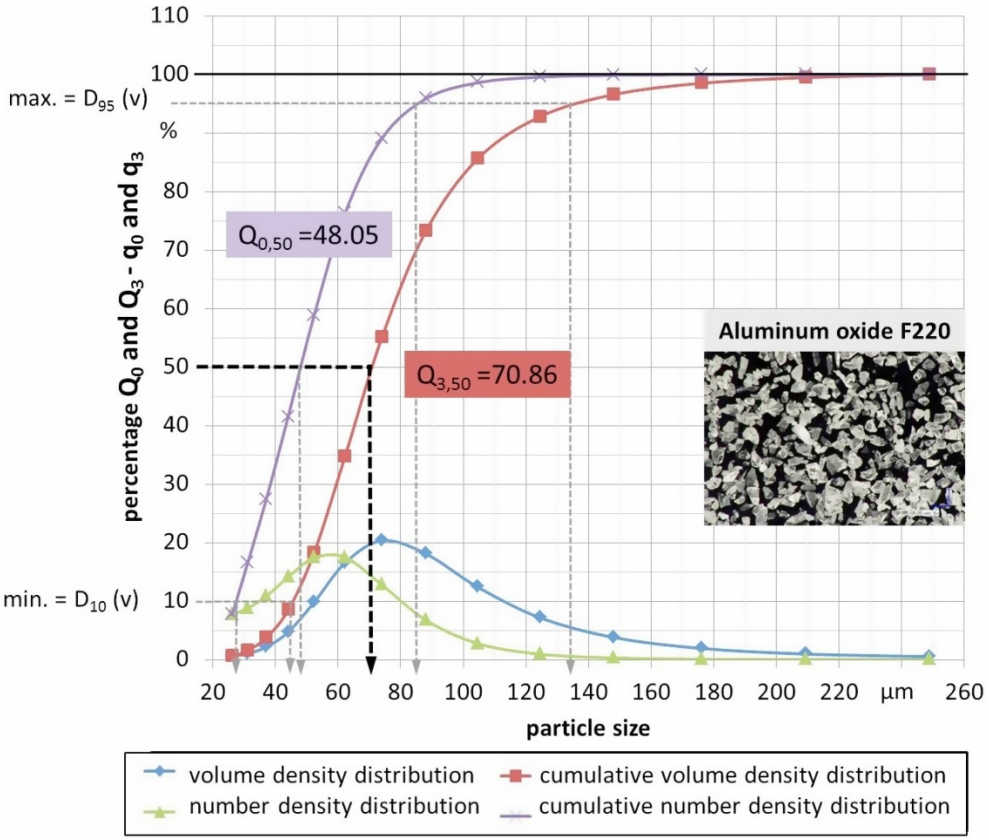

Figure 2: Number and volume distribution F220

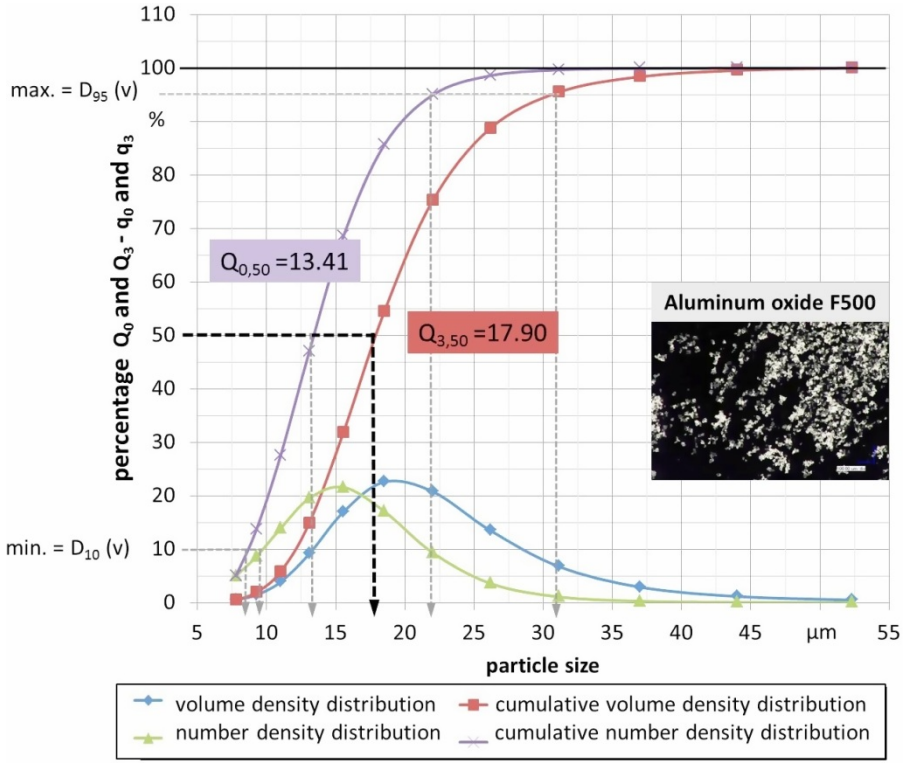

Figure 3: Number and volume distribution F500

In order to compare the manufacturer's instructions to the measured data, a statistical evaluation of particle size was conducted for the smallest, D_{10}, the middle, D_{50}, and the largest, D_{95}, (*Figure 4*). F500 is the most homogeneous, then comes F220.

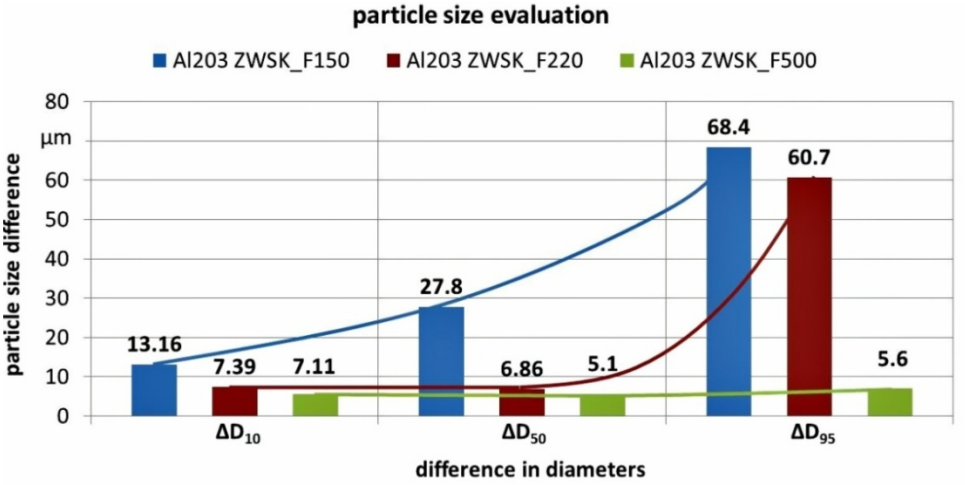

abrasive particle type	manufacturers instructions			measured data			particle size difference		
	D_{10}(v) in µm	D_{50}(v) in µm	D_{95}(v) in µm	D_{10}(v) in µm	D_{50}(v) in µm	D_{95}(v) in µm	ΔD_{10} (v) in µm	ΔD_{50} (v) in µm	ΔD_{95} (v) in µm
Al_2O_3 ZWSK_F150	63.0	84.5	106.0	76.16	112.3	174.4	**13.16**	**27.8**	**68.4**
Al_2O_3 ZWSK_F220	53.0	64.0	75.0	60.39	70.86	135.7	**7.39**	**6.86**	**60.7**
Al_2O_3 ZWSK_F500	5.0	12.8	25.0	12.11	17.90	30.60	**7.11**	**5.1**	**5.6**

Figure 4: Statistical evaluation of particle size

To understand the properties of the particles is necessary for the control of dispersed systems. Generally, the particle geometry, shape, surface roughness and porosity are the key properties. In the simplest case a spherical shape is assumed and the diameter characterizes the particle [Boh04] but, unfortunately, particles mostly exhibit distinct irregular shapes. That makes finding a characteristic measure of particles very difficult [Sti09]. For the identification of the particle shapes, *Walz* suggested to determine the largest and smallest dimensions from 30 grains in the orthogonal spatial coordinates [Wal36]. An average of the ratios X_b/X_c and X_a/X_c is calculated and the particles are roughly classified (*Figure 5*). Sphere like particles can be characterized by an equivalent diameter with the following major variables:

d_v Diameter of the sphere with identical volume,

d_s Diameter of the sphere with identical surface,

d_a Diameter of the sphere with identical cross-sectional surface,

d_w Diameter of the sphere with identical descent velocity.

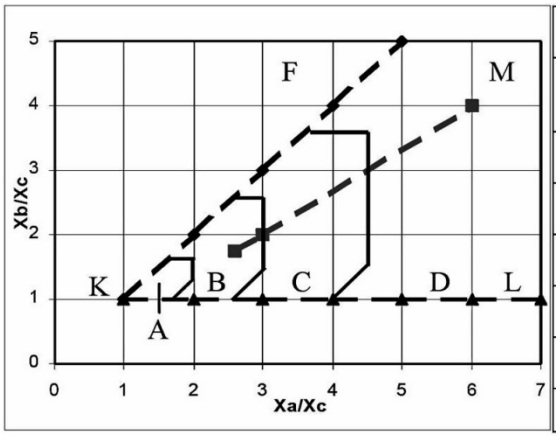

A	spherical, polygonal, penetrated to cubic grains
B	still penetrated appearing grains, which differ but far away from being spherical
C	flat and long-shaped grains
D	extremely flat and long grain
L	length limit
F	flatness limit
M	theoretical boundary between flat and long form
K	definitely cubic

Figure 5: Form diagram by Walz [Wal36]

If the particles show irregular shapes as in our study, the sphericity ψ can be calculated with the equivalent diameters d_v and d_s according to the equation (2).

$$\Psi = \frac{\pi d_v^2}{\pi d_s^2} = \left(\frac{d_v}{d_s}\right)^2 \tag{2}$$

Relations between the characteristic diameters and ψ which is valid for concave particles can be given as in equation (3), and only d_w is associated with Stokes field.

$$d_v = d_s \Psi^{1/2} = d_a \Psi^{1/2} = d_w \Psi^{-1/4}. \tag{3}$$

Table 2 shows sphericity values of regular and irregular particles. In our studies we adopted the form factor ≈ 0.6 corresponding to the sphericity of "edged" particles, for calculations of particle volumes.

Table 2: Form factors [Buh88]

Irregular particles	Ψ	Regular Particles	Ψ
rounded	≈ 0.8	**sphere**	= 1
angular, sand, potash	≈ 0.7	**cube**	= 0.806
edged	≈ 0.6	**cylinder, slice**	$= \frac{h}{2h+D_R}\left(18\frac{D_R}{h}\right)^{1/3}$
flat	0.4 – 0.5	**tetrahedral**	= 0.67

The particle mass was calculated according to the volume and the density of the particles, see *Table 3*. Essential properties of the abrasive medium can be determined

with respect to the particle size distribution so we can estimate the quality of the grain and the quality of the jet. Since the abrasive particles have a very fine grain and tend to agglomerate, it is very important to characterize the operational behavior of the particles.

Table 3: Calculated particle mass

Particle Types	ZWSK_F150	ZWSK_F220	ZWSK_F500	Units
D10 (v)	76.16	60.39	12.11	**µm**
D50 (v) median	112.3	70.86	17.90	**µm**
D95 (v)	174.4	135.7	30.60	**µm**
Density	4.00	4.00	4.00	**kg/m³**
Volume	3.46E-04	8.70E-05	1.40E-06	**m³**
Mass	**1.39E-12**	**3.48E-13**	**5.61E-15**	**kg**

2.2 Particle characterization

Figure 6 shows the schematic design of the abrasive water jet with injector method and the optical laser measuring method which is used to analyze the particle velocity in the abrasive air jet with a contactless optical laser technology. The employed nozzle has a diameter d_0 = 1 mm and an input pressure of p = 2.5 bar. The carrier medium air and particles are mixed in the mixing chamber of the nozzle and the particles are pushed through the nozzle by air. The horizontal distance from the high-resolution digital camera to the center of the nozzle diameter is l = 250 mm for the measurements. The flow was enlightened with a double pulsed flashing laser and was recorded with the digital camera. The measured data and the images were directly transferred to the computer for analysis.

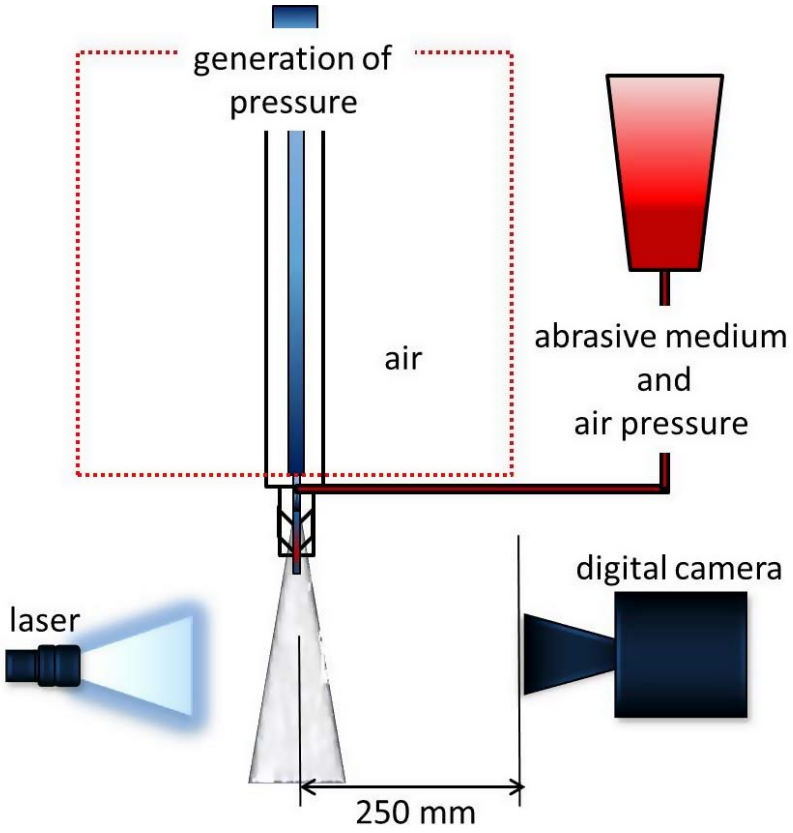

Figure 6: Model of the experimental rig

The abrasive medium F500 which was the most homogenous according to the particle size analysis, exhibited a disadvantage in experiments: There was a cloudy mist of dust with a non-uniform diffuse pattern during jet blasting. Moreover, the adhered particles caused clogging due to the assumed porosity. In practice, especially in the nanometer range, this behavior is commonly observed. The adhesive forces grow compared to the inertia forces according to the porosity of particles. Therefore, particles remain in agglomerated position and fall into deeper holes so other holes remain unfilled [Sti09]. The porosity of Particles ε_p in equation (4) is the ratio of the total volume of cavities V_{HP} to the total particle volume V_p, and is then present when the cavities are located in interior of the individual particles [Sti09].

$$\epsilon_p = \frac{V_{HP}}{V_p} \tag{4}$$

In order to avoid the agglomeration of particles, a high pressure may be used but that is against our machining process, deburring by low pressure abrasive water jet blasting. Thus, the abrasive medium F500 is unsuitable for our deburring process. The burr size and the burr foot width on micro workpieces are other important criteria for the selection of the abrasive medium. Compared with those measured burr feet width

by Biermann which are between 12 microns and 39 microns, the abrasive medium F150 with a volume diameter D_{50} = 112 microns is too large hence unsuitable for our process, see *Figure 7*, [Bie12]. There is a risk that the material is embedded instead of being removed and the surface is damaged by the strong abrasive action.

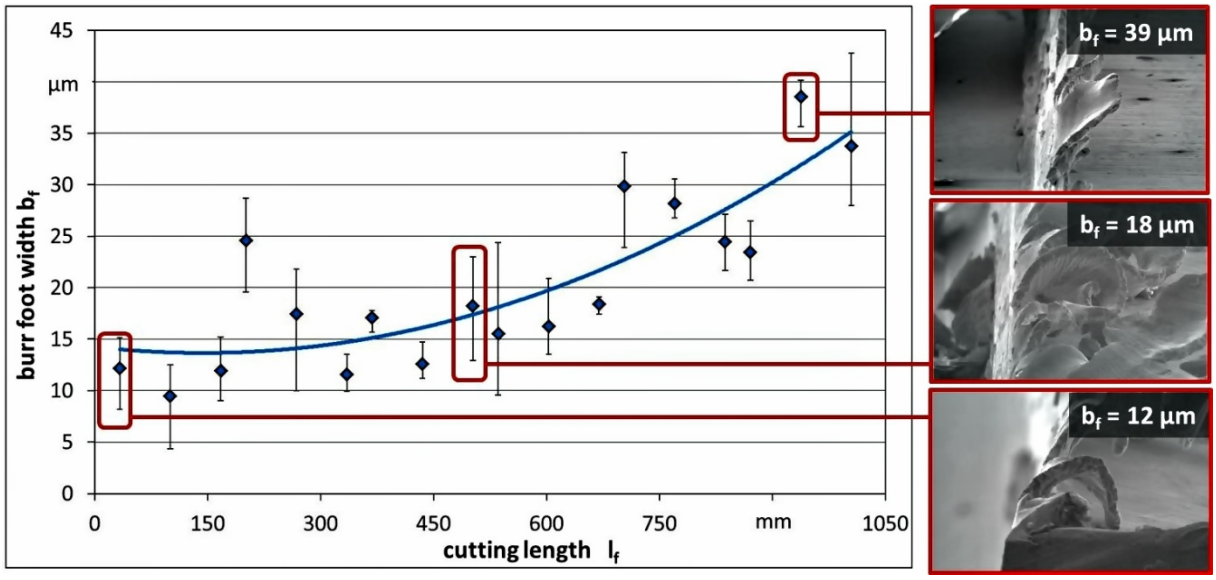

Figure 7: Measured burr foot width

The wide particle size distribution of the abrasive medium F220 has the advantage that the porosity is reduced and the particle distribution in the dispersed system yielded the desired uniform pattern and was used in our experiments, cf. *Figure 8*.

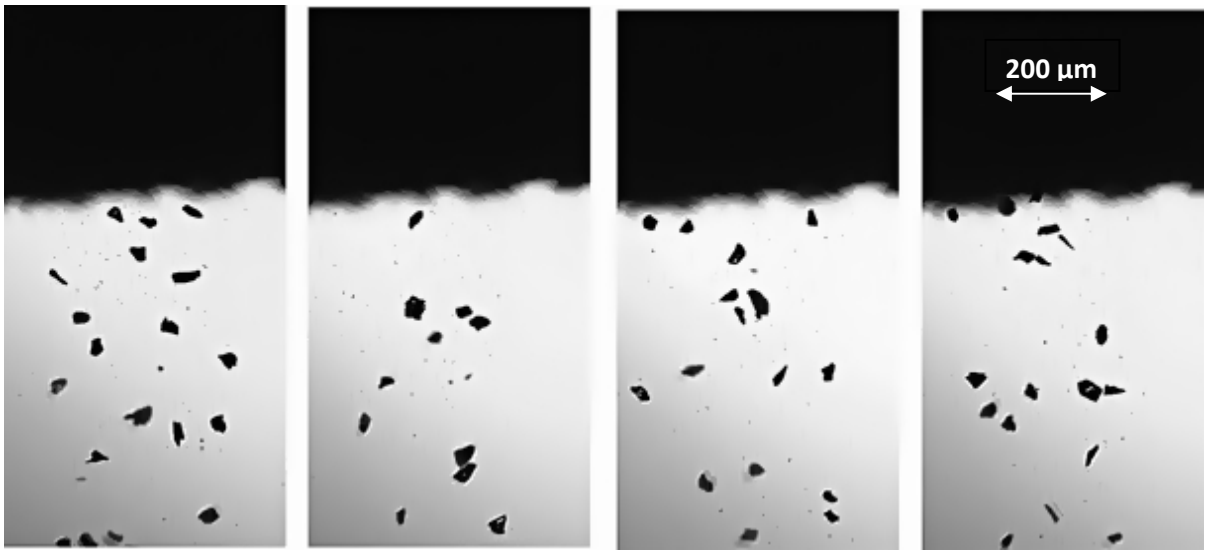

Figure 8: Particle distribution in abrasive air jet

3 Numerical simulations

In technical systems the single-phase laminar free jet is hardly used for any application but studying single-phase laminar free jets is useful to understand the possible simplest case; the velocity field can be calculated according to the boundary layer equations [Sch97]. In order to gain an estimate of the velocity field in two-phase free jets, *equation (5) - (10)* are used. The Reynolds number (*Re*) is regarded as the key parameter and described with the equation (5) with the characteristic length being the nozzle diameter d_0 and the transport speed U in the nozzle.

$$Re = \frac{U\, d_0}{v} \tag{5}$$

The transport speed U is obtained according to equation (6).

$$U = \frac{4\, \dot{V}}{d_0^2\, \pi} \tag{6}$$

In order to approximately describe the turbulent velocity profile $u(r)$, a simple formula is employed, equation (7).

$$\frac{u(r)}{U_{max}} = \left[1 - \frac{2r}{d}\right]^{\frac{1}{n}} \tag{7}$$

Here, the exponent n depends on the Reynolds number and is approx. 7. Therefore, the model is also known as 1/7 power law. The derivative of the velocity with respect to the radius at the center should be zero but it is finite; hence, there exists a "pointed arch". Newtonian shear stress law is used in accordance with equation (8) so that the slope is finite at the edge.

$$\tau = \mu \frac{du}{dr} \tag{8}$$

The fluid is subject to the shearing effect at the outlet and gains a rotational motion. These results in a low turbulent flow with very small vortices which are formed due to the mixing of the jet with the surrounding fluid are not visible. This effect is also known as "entrainment effect". The width b of the jet grows with time t and is proportional to the maximum velocity U_{max} and can be calculated according to equation (9).

$$\frac{Db}{Dt} \propto U_{max.} \tag{9}$$

In the stationary case the time derivative vanishes, and the velocity becomes proportional to only the derivative of width with respect to height; then, the equation (10) can be applied.

$$U_{max} \frac{db}{dy} \propto U_{max} \tag{10}$$

Since the dispersed two-phase free jet flow cannot be analytically described, it requires computational fluid dynamics (CFD) simulation. CFD software packages can be successfully used for simulations [Flu98]. Free jet flows with relatively low particle loads are usually numerically simulated according to the Euler-Lagrange approach [Gill00]. Once the loading is higher and particle-particle interactions must be taken into account, numerical simulations become arguable. Thus, further experimental and numerical investigations must be performed in order to develop better models and to verify existing ones [Gill00].

Flow dynamics in the numerical simulations were described by the Navier-Stokes equations. In order to characterize the turbulent flow and to close the arising mathematical equations, the two-equation *k-ε* turbulence model was adopted and the appropriate boundary conditions were provided. *Figure 9 (left)* shows the ranges over which the abrasive pressure air free jet spreads. 45 measurement fields that were built up with a 30x30 matrix for each were considered. The velocity variation and the corresponding particle distribution were visualized according to the jet length and width on the basis of the measurement data with a standard application; cf. *Figure 9 (center)*. Subsequently, a CFD simulation model was created using the measurement results, cf. *Figure 9 (right)*. The comparison of the analytical and simulation results shows a good agreement for the flow field or velocity profile.

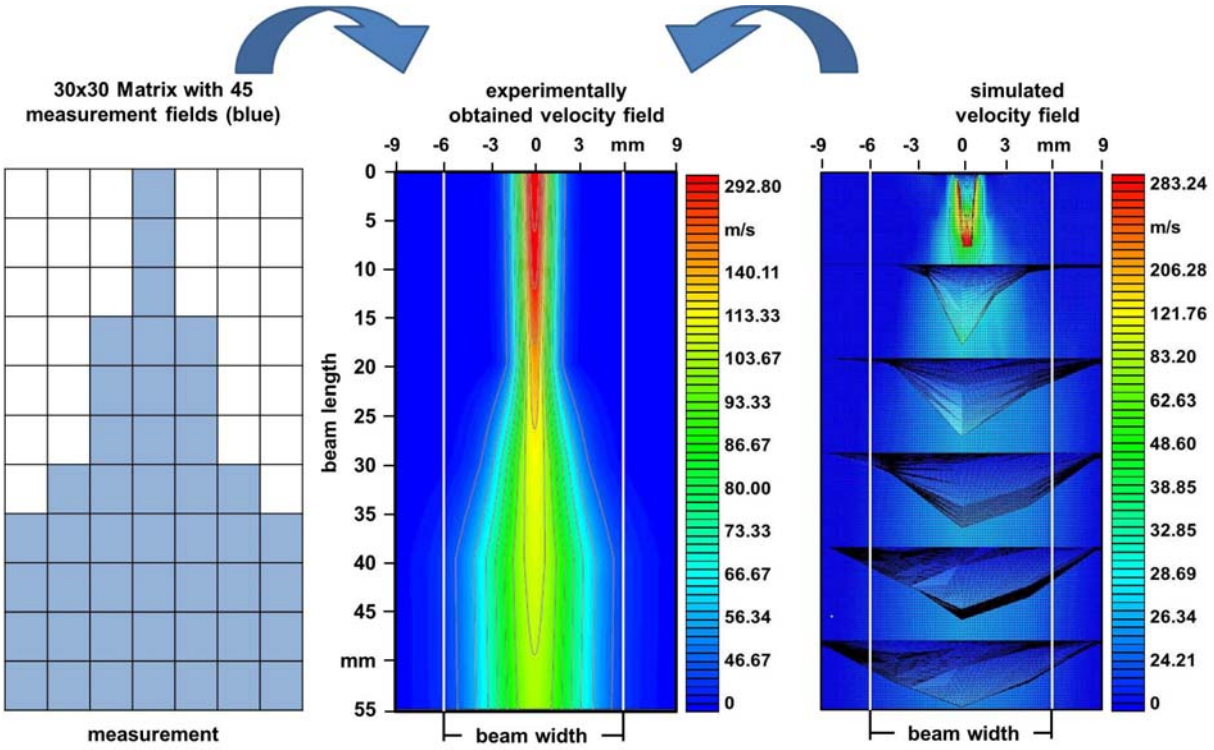

Figure 9: Flow field: Experimental grid (left), evaluated measured data (middle) and simulation (right)

The particle distribution remains unchanged for some distance along the axis but later due to the expansion of the jet, the particles spread out, i.e. the number density of particles immediately decreases when the jet expands (*Figure 10*).

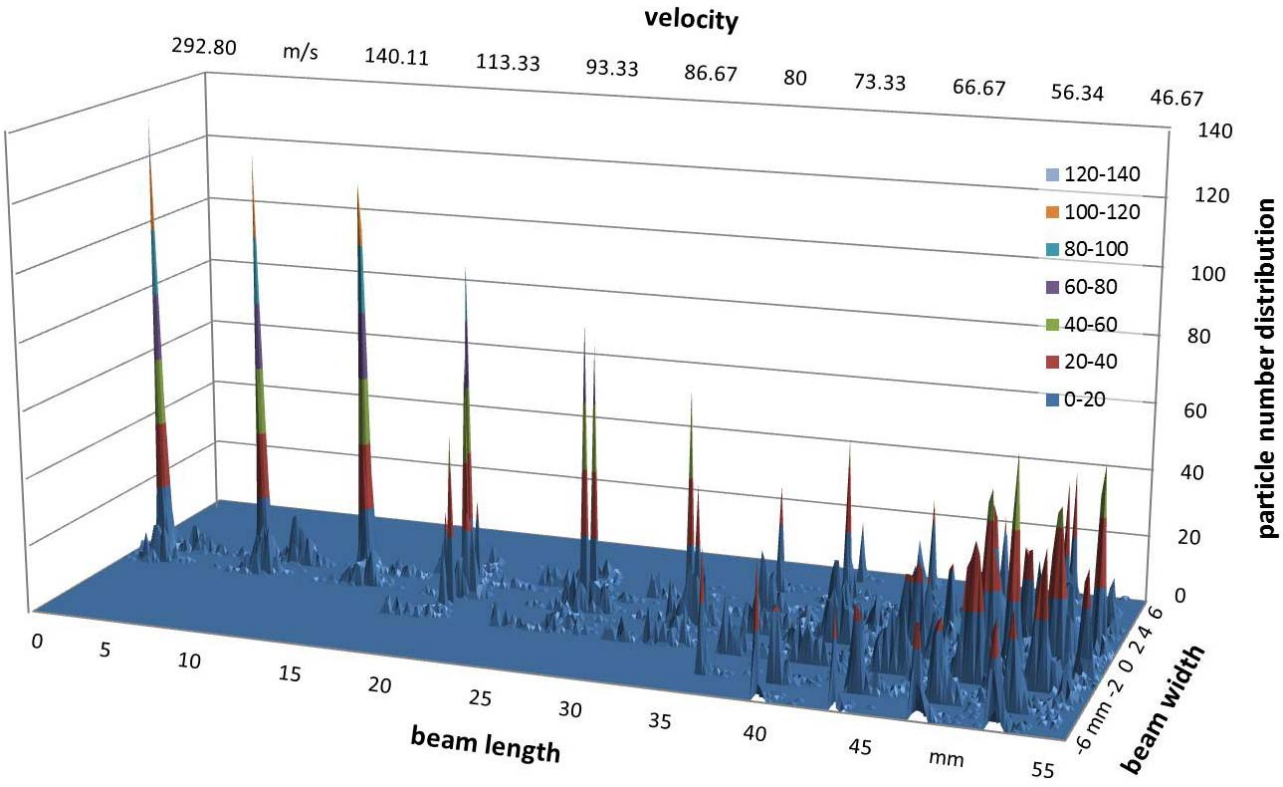

Figure 10: Velocity field - particle number distribution on jet length and width

The interaction between the particles and the turbulent jet flow causes a strong rotational motion of the particles, especially for the larger ones. Hence, the momentum transfer from air to particles does now not only result in translational motion but rotational motion, as well; the particles decelerate more quickly than in air, cf. *Figure 11*.

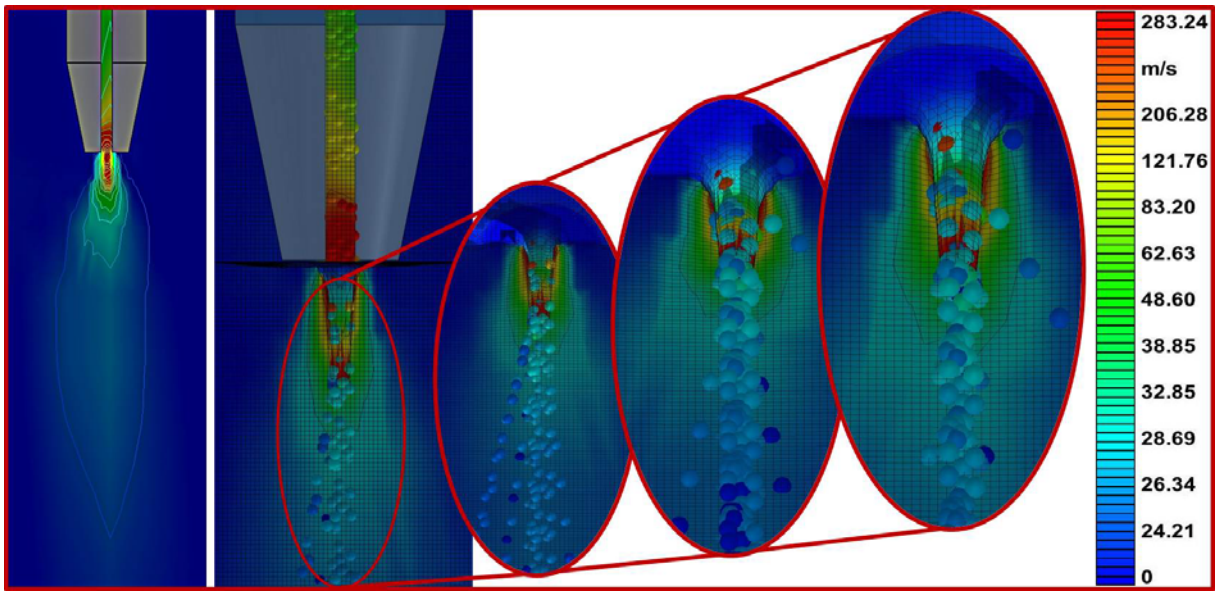

Figure 11: Simulated velocity field and simulated particle distribution in abrasive air jet

4 Discussion

The developed velocity profiles at the outlet which are obtained according to the empirical formulae, numerical simulations and measurements are shown in *Figure 12*. The flow profile which is computed by numerical simulations is more trapezoidal compared to the other two and all three exhibit a turbulent profile. The calculated value of v_{max} with empirical formulae and numerical simulations are 284.1 m/s and 283.2 m/s respectively. These values are consistent with the measured value of 282.9 m/s. The numerical simulations are not yet grid independent and can be performed on a finer grid; the parameters in the numerical simulation can be finely tuned so that the numerical simulation will be more accurate and closer to the experiments. As a summary, CFD simulations will be satisfactory and can be considered as a reference result if a sufficiently fine grid is used, a more appropriate turbulence model is employed, proper boundary conditions are imposed, and the boundary layer is treated with a more accurate numeric; even though our numerical results are acceptable with less than % 3.5 deviations.

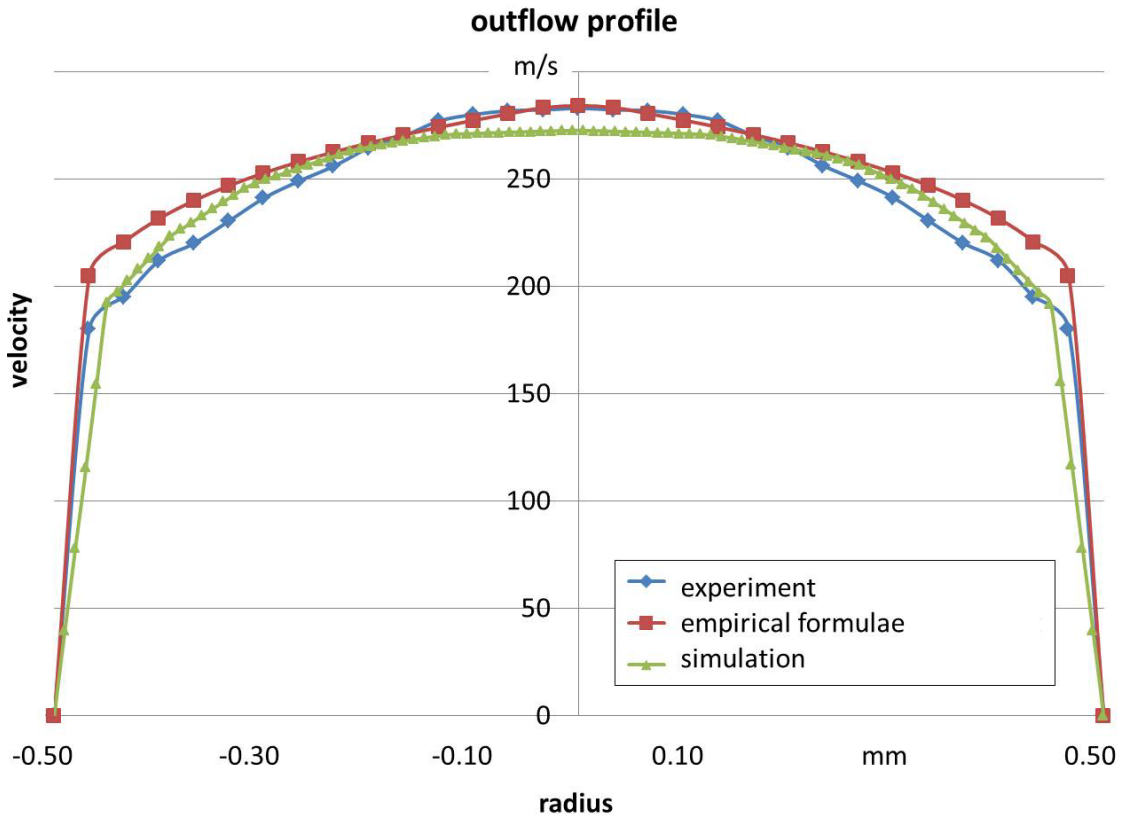

Figure 12: Velocity profile at the outlet along the radial direction

The maximum velocities which are obtained at 5 mm intervals for 55 mm along the axis of the jet with experiments, empirical formulae and CFD simulations are compared, cf. *Figure 13*. The velocity profile gets wider and flatter because the jet penetrates to the surrounding air, expanding the maximum velocity decreases along the jet axis.

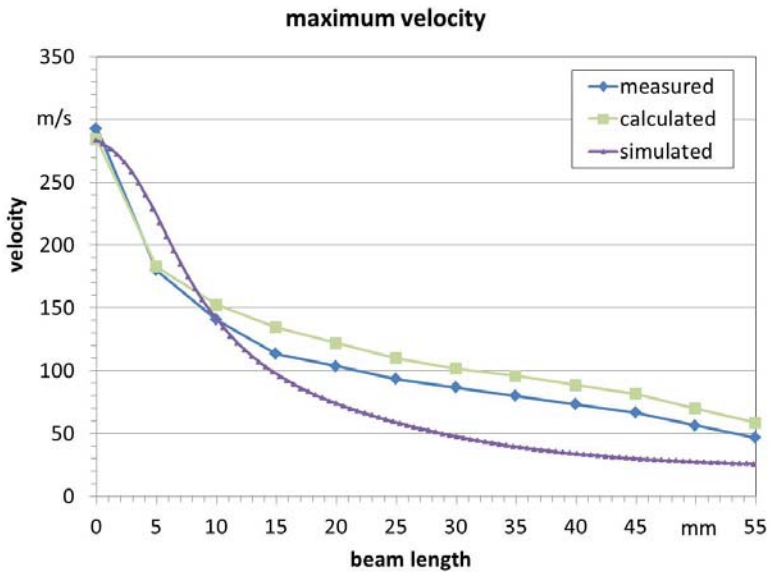

jet in mm	v_{max} measured in m/s	v_{max} calculated in m/s	v_{max} simulated in m/s
0 - 5	292.80	284.11	283.24
5-10	180.11	182.78	258.20
10-15	140.64	152.63	206.28
15-20	113.33	134.52	121.76
20-25	103.67	122.08	83.20
25-30	93.33	110.08	62.63
30-35	86.67	101.68	48.60
35-40	80.00	95.78	38.98
40-45	73.33	88.62	32.85
45-50	66.67	81.73	28.69
50-55	56.34	69.99	26.34
55-60	46.67	58.47	24.21

Figure 13: Maximum velocities: Measurements, calculated results with empirical formulae and CFD simulations

The viscous forces are very influential: The unsteady jet strongly interacts with the surrounding air. The viscous forces cause dissipation of the jet's energy; additionally, the energy is transferred to the surrounding air [Sig07]. The jet's energy and velocity decrease with the increasing jet-length, so do the particles'. In addition to the particle mass the measured, calculated and simulated maximum- and averaged-values of the velocity and of the kinetic energy are shown in *Table 4*.

Table 4: Summary of the results for velocity and kinetic energy

ZWSK_F220	Measured	Calculated	Simulated	Units
Mass	3.48E-13	3.48E-13	3.48E-13	**kg**
Maximum velocity	292.80	284.11	283.24	**m/s**
Average kinetic energy	2.15E-09	2.66E-09	1.78E-09	**kg·m²/s²**
Maximum kinetic energy	1.49E-08	1.40E-08	1.40E-08	**kg·m²/s²**

Conclusions

As a result of the particle classification, a suitable abrasive medium, F220, is determined for the novel deburring process; furthermore, initial input variables such as particle shape, particle size, particle mass, particle velocity and the kinetic energy can be determined for simulations with a material removal model. The CFD simulations, the measured data and the calculated results according to the empirical formulae are shown to be acceptably agreeing. A good pre-optimization can be achieved by using the CFD simulations in parallel to experimental studies so that the effort and the cost in development significantly decrease. In order to improve the quality of the numerical simulations, the turbulence model should be tuned further and simulations should be performed on a finer grid. Moreover, measurements with special methods for real abrasive waterjet are also planned. Based on the comprehensive CFD simulations, the flow field in abrasive waterjets can be accurately resolved, and the results can be safely used in simulations of the surface erosion. In addition to the CAE based development process, a design of experiments for the system characterization should be carried out. Our outlook is to develop a novel deburring process, namely low pressure abrasive water-jet blasting, by obtaining explicit values of major variables, determining dependencies of variables and building a novel simulation model.

Acknowledgements

The Institute of Machining Technology and the Institute of Applied Mathematics (LS3) thank the Deutsche Forschungsgemeinschaft for the provision of subsidies as part of the DFG project "Development and validation of a simulation approach for deburring of micro-structured shape memory components by abrasive water-jet blasting" (DFG GZ: BI 498/32-1, TU 102/39-1).

Das Institut für Spanende Fertigung und das Institut für Angewandte Mathematik (LS3) danken der Deutschen Forschungsgemeinschaft für die Bereitstellung von Fördermitteln im Rahmen des DFG-Projektes „Entwicklung und Validierung eines Simulationsansatzes zum Entgraten mikrostrukturierter Formgedächtnisbauteile durch Abrasivwasserstrahlen“ (DFG GZ: BI 498/32-1, TU 102/39-1).

References

1. Letter

[Bie12] D. Biermann, E. Özkaya, *VDI-Z Integrierte Produktion* **2012**, *154*,70.

[Baa96] R. Baar, W. Riess, *Journal of Flow Measurement and Instrumentation* **1997**, 8, 1.

2. Dissertations

[Gill00] Gillandt, I. : *Analyse der Turbulenzmodulation im dispersen zweiphasigen Freistrahl*, Universität Bremen, Shaker Verlag Aachen, **2000.**

3. Books

[Boh04] Bohnet M. (Hrsg): *Mechanische Verfahrenstechnik*, Wiley-VCH, **2007**, S.13.

[Him93] Himmelreich, U.: *Fluiddynamische Untersuchungen an Wasserabrasivstrahlen*, VDI Fortschrittsberichte, Reihe 7: Strömungstechnik, Nr. 219, VDI-Verlag, Düsseldorf, **1993.**

[Les74] Leschonski, K.; Alex, W.; Koglin, B.: *Teilchengrößenanalyse*, Chem.-Ing.-Techn. 46 (**1974**), S. 23-26.

[Sch97] Schlichting, H.: *Grenzschicht- Theorie*, 9. Auflage, Springer, Berlin,**1997**

[Sig07] Sigloch, H.: *Technische Fluidmechanik*, Springer Verlag 2007, S. 106-107.

[Spu87] Spur, G.; Felsing, W.; Gutsche, C.: *Robotergeführtes Trennen mit Hochdruckwasserstrahl und Abrasivmittelzusatz*, ZWF 82 (**1987**) 11, S. 568-572.

[Sti09] Stiess, M.: *Mechanische Verfahrenstechnik – Partikeltechnologie 1*, Springer Verlag **2009**, S.63, 66.

[Wal36] Walz, K.: *Die Bestimmung der Kornform der Zuschlagstoffe*, Betonstraße 11, **1936,** S.27-32.

4. International Conference

[Mea03] P.S. Coray, B. Jurisevic, M. Junkar, K.C. Heiniger: *Measurements on 5:1 scale abrasive water jet cutting head models, Proceedings of the 6th International Conference on Management of Innovative Technologies MIT'2003*, Piran, Slovenia, 13-14 October **2003**, S.87-102

5. Other

[Flu98] *Fluent User Guide*, Fluent Inc., Lebanon, USA, July **1998**